

Phase sensitive parametric optical metrology: Exploring the limits of 3-dimensional optical metrology

Richard M. Silver*, Jing Qin, Bryan M. Barnes, Hui Zhou, Ronald Dixson, and Francois Goasmat
Semiconductor and Dimensional Metrology Division, Physical Measurement Laboratory
National Institute of Standards and Technology
100 Bureau Dr. MS 8212, Gaithersburg, MD USA 20899-8212

ABSTRACT

There has been much recent work in developing advanced optical metrology applications that use imaging optics for critical dimension measurements, defect detection and for potential use with in-die metrology. Sensitivity to nanometer scale changes has been observed when measuring critical dimensions of sub-wavelength features or when imaging defects below 20 nm using angle-resolved and focus-resolved optical data. However, these methods inherently involve complex imaging optics and analysis of complicated three-dimensional electromagnetic fields. This paper will develop a new approach to enable the rigorous analysis of three-dimensional through-focus optical images. We use rigorous electromagnetic simulation tools and statistical methods to evaluate sensitivities and uncertainties in the measurement of three dimensional layouts encountered in critical dimension, contour metrology and defect inspection.

Keywords: Optical metrology, electromagnetic simulation, evaluate sensitivities and uncertainties, phase sensitive measurements, through-focus three-dimensional field.

1. INTRODUCTION

Success in developing advanced optical metrology methods that use imaging optics for critical dimension (CD) measurements, overlay metrology, and defect detection has in part been based on the analysis of phase and scattered frequency information available when using image-based systems. For some time it has been shown that sensitivity to nanometer scale changes can be observed when measuring critical dimensions of sub-wavelength features or when imaging defects below 20 nm using angle-resolved and focus-resolved optical data [1,2]. There are many advantages to using low cost high-throughput optical tools. However, these methods inherently involve complex imaging optics and analysis of complicated three-dimensional scattered electromagnetic fields.

We have previously used optical imaging methods in a scatterfield platform to perform what are essentially angle-resolved scatterometry measurements on a high magnification imaging platform [3,4]. These measurements were focused on acquiring images as a function of angle for dense linewidth arrays that fill the field of view (FOV), using targets similar to those used in scatterometry. These measurements were analyzed with rigorous regression methods with uncertainties calculated. Prior to these measurements, attempts were made to model images and line profiles acquired through focus [5,6]. This required modeling the complete 3-dimensional electromagnetic field. Data were acquired through focus and successful quantitative agreement between theory and experiment was not achieved. This was largely due to two primary shortcomings. First, detailed tool functions needed to be developed that normalize and correct for the illumination and collection optical path errors that independently have a direct impact on the resulting images. The second effect to be recognized is that even in the nominally simplest single plane wave illumination example, the scattered light from any finite target has a large range of spatial frequencies that need to be accurately normalized and modeled.

Acceptable quantitative statistical analysis with rigorous agreement between experiment and theory would represent an important advance in image-based optical metrology. It could provide a means for CD metrology of very small sub-field targets. The measured fields could also be non-repetitive and irregular structures unlike those required for scatterometry. However, a key to the success of scatterometry has been the ability to model measurements with an acceptable degree of accuracy and to quantitatively address parametric correlation in measurement uncertainty.

Here we present a new approach that enables the rigorous analysis of three-dimensional through-focus and angle-resolved optical images. These imaging methods sample the three-dimensional electromagnetic fields above the sample

or target of interest. The technique involves parametric fitting of the discretized three-dimensional scattered field and allows for the quantitative evaluation of correlation effects due to fitting parameters such as side wall, feature profile and etch depth. Using this approach it becomes possible to perform dimensional measurements of in-die layouts through imaging and analysis of high order three-dimensional optical fields.

In this paper we use rigorous electromagnetic simulation tools and statistical methods to evaluate sensitivities and uncertainties in the measurement of two and three dimensional layouts encountered in critical dimension, contour metrology and defect inspection. We first perform a simulation study to develop the basic understanding of possible measurement sensitivities and uncertainties. This section of the paper is intended to give a realistic evaluation of possible experimentally achievable sensitivities using a realistic instrument and sample noise model.

To develop rigorous analysis of optical imaging data using both theoretical and experimental methods, comprehensive and quantitative characterization of the optical metrology tool is necessary. To facilitate rigorous phase sensitive measurements of the through-focus three-dimensional field data, illumination engineering and sophisticated tool normalization are needed, including an appropriate hardware platform that provides access to a conjugate back focal plane giving full angular control of the optical path.

2. HARDWARE PLATFORM AND REGRESSION ANALYSIS

The scatterfield microscopy technique, which provides full access and control of the angular distribution of light, has been described in detail elsewhere [7, 8]. The basic instrument is based on a Köhler illuminated bright field microscope with a large accessible conjugate back focal plane (CBFP). Data are acquired as a function of angle or focus position as illustrated graphically in Figure 1. A charge coupled device (CCD) image is captured at each angle or focus position. The images are then stored as arrays as a function of angle or focus position. The intensity images generally include a specular reflection component and higher order diffracted light.

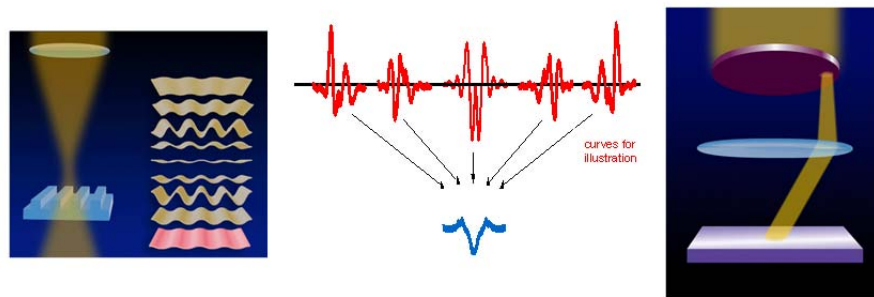


Figure 1. Schematic of the experimental methods for focus-resolved and angle-resolved data acquisition. (left) Information about the target can be collected at various through-focus positions. (center) The use of a low illumination numerical aperture (NA) with incoherent illumination is often preferred to using a large NA which combines the profiles and smears out information content. (right) specific angles of light can be directed at the surface by engineering the CBFP.

We now develop the nonlinear regression model for application to a set of images. Although the model can be expanded to a hybrid metrology approach to include *a priori* information using a Bayesian approach, we only employ a single measurement tool in this paper. Only an overview to the initial derivation is given here, see Refs. 4 and 9 for a more detailed formalism.

In general a complete set of measurements consists of N sets of data points acquired under a varying set of conditions for both simulations and experimental measurements. Each set of data points corresponds to an image profile at a given angle and focus position. There are K model parameters expressed as a vector $\mathbf{a} = \{a_1, \dots, a_K\}$, and represent the model input parameters, for example, CD, sidewall, height, illumination angle and focus position. We have N sets of measured values of Y denoted as $\{y_1, \dots, y_N\}$ and N simulated sets of values $y(x_i; \mathbf{a})$ corresponding to the i^{th} data point

x_i . We want to compare the measured values $\{y_1, \dots, y_N\}$ with the simulated values $\{y(x_i; \mathbf{a})\}, i = 1, \dots, N\}$ and find an optimal estimator of the parameter vector $\mathbf{a} = \{a_1, \dots, a_K\}$.

Following reference [10], using a first-order Taylor expansion, a linear approximation of the nonlinear regression is given by

$$y_i = y(x_i; \mathbf{a}(0)) + \sum_{k=1}^K \left[\frac{\partial y(x_i; \mathbf{a})}{\partial a_k} \right]_{\mathbf{a}=\mathbf{a}(0)} (a_k - a_k(0)) + \varepsilon_i, \quad (2)$$

where $\mathbf{a}(0) = \{a_1(0), \dots, a_K(0)\}$ is an initial value or an optimal value of \mathbf{a} and ε_i is the corresponding random error with zero mean [11]. By re-parameterization, the model can be expressed as

$$y_i(0) = \sum_{k=1}^K D_{ik}(0) \beta_k(0) + \varepsilon_i, \quad (3)$$

with

$$D_{ik}(0) = \left[\frac{\partial y(x_i; \mathbf{a})}{\partial a_k} \right]_{\mathbf{a}=\mathbf{a}(0)}, \quad (4)$$

and $\beta_k(0) = a_k - a_k(0)$ and $y_i(0) = y_i - y(x_i; \mathbf{a}(0))$, see Ref. 11. The covariance matrix of the experimental values $\{y_1, \dots, y_N\}$ is denoted by $\mathbf{V} = \text{diag}[\sigma_1^2, \dots, \sigma_N^2]$.

In the regression approach outlined above, we concatenate the data strings from each profile and then solve for the best parameter fit and parametric uncertainties as we have previously outlined.

The following noise profiles were used in the simulations.

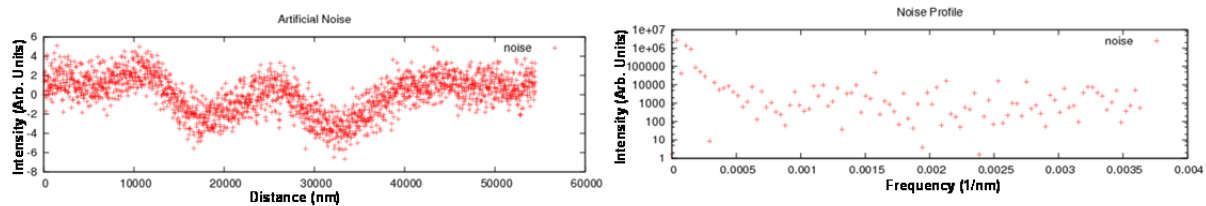


Figure 2. Examples of the noise profile and frequency distribution used in the simulation study.

Two different types of samples are analyzed in this paper. We use a continuous array of lines with 100 nm CD and 600 nm pitch which is referred to as the L100P600 target. We also used dense, finite arrays of lines with either 100 nm CD and 300 nm pitch or 50 nm CD and 175 nm pitch, which are referred to as L100P300 and L50P175, respectively. Each type of target is printed using a focus exposure matrix (FEM) providing a series of die with linewidth and sidewall profiles that vary on the nanometer scale. The L100P600 target fills the FOV and results in an optical scattering response with well defined frequency content due to specific diffraction orders. The L100P300 and L50P175 targets on the other hand only fill a portion of the FOV and as finite structures have edges present that scatter a broad range of spatial frequency information.

The L50P175 line array has approximate printed middle width values of 35 nm based on atomic force microscopy (AFM) measurements. The starting point parameters used to characterize the line geometry are based on AFM values.

The AFM is used to acquire line width profiles, pitch, and height which serve two purposes. First, the AFM values are used as the initial starting point for the simulation library [12]. In this application the AFM is used to define the approximate space of the simulation domain. For the second use, the AFM values are used as reference values to compare with the optical fitting data results based solely on the above described regression routines.

3. SIMULATION STUDIES

Simulation studies were carried out for a range of line width and pitch values. This simulation component of the paper was performed similarly to previous published simulation studies whereby an n-dimensional parameter space is simulated with an appropriate density of simulations [13]. A curve or data set is taken from a central location in the space and noise as described above is added to the simulated profile or set of profiles. This noise laden simulation set is then treated as the “experimental” data set to be fit. As seen in the data that follow, a substantial and realistic noise model is used. Some of the parameter choices overlapped the experimental data from the experimental section of this paper. Our scattering simulation methods include a finite difference time domain (FDTD) approach and a rigorous coupled waveguide analysis model (RCWA) both of which were developed in house and previously published [14]. The in house model development is important as significant advances of the Fourier optical simulation components were required.

In Figure 3, on the left, is shown the nominal target geometry including the CD, number of lines and the pitch as well as the macro-pitch. The macro-pitch is the period over which the finite grating is repeated in the numerical simulations while the lines are infinite in length for these simulations. In the center part of the figure examples of the simulated “experimental” curves are overlaid with the best fit curves from the simulated library. On the right the standard fitting uncertainties in the fits are shown for the four floated parameters for both through-focus and angle-resolved analysis. The uncertainties are 1σ . These data are for the L100P300 finite arrays in the upper portion and L50P175 in the lower part of the figure. These particular targets are chosen to be large enough that the array edges are “isolated” from one another such that the central region reaches its nominal steady state optical response for an infinite array. This is done to enable modeling comparison of the edges of a finite scatterometry target, as well as a base line calibration for both the nearby substrate and the dense specular or high order optical response from the arrayed line region.

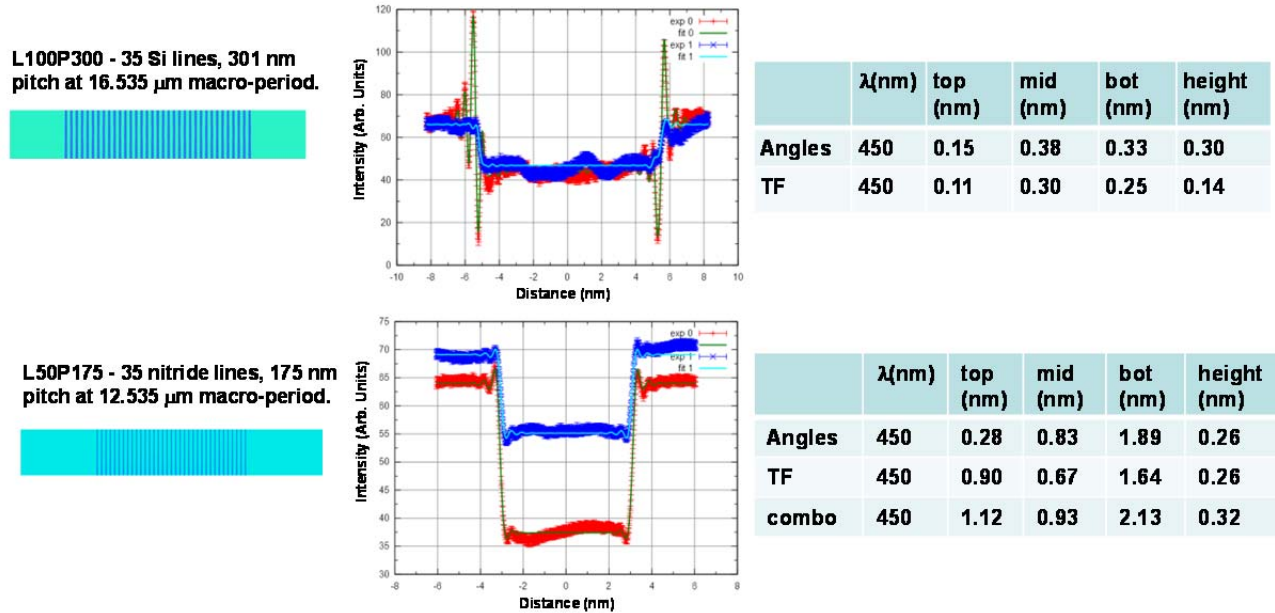


Figure 3. Each angle or through-focus scan consists of 84 profiles. The graphics each show best fit simulation curves and “simulated experimental curves” for two polarizations at a selected focus or angle position. Combining some angle and through focus (TF) scans (78 profiles) does not reduce the parametric uncertainties.

Additional simulation studies are shown in Figure 4 to investigate much smaller, industrially relevant dimensions. Here, 9 nm CD lines at a 32 nm pitch and 160 nm pitch are used to investigate lithographically dense and isolated features anticipated in future manufacturing generations.

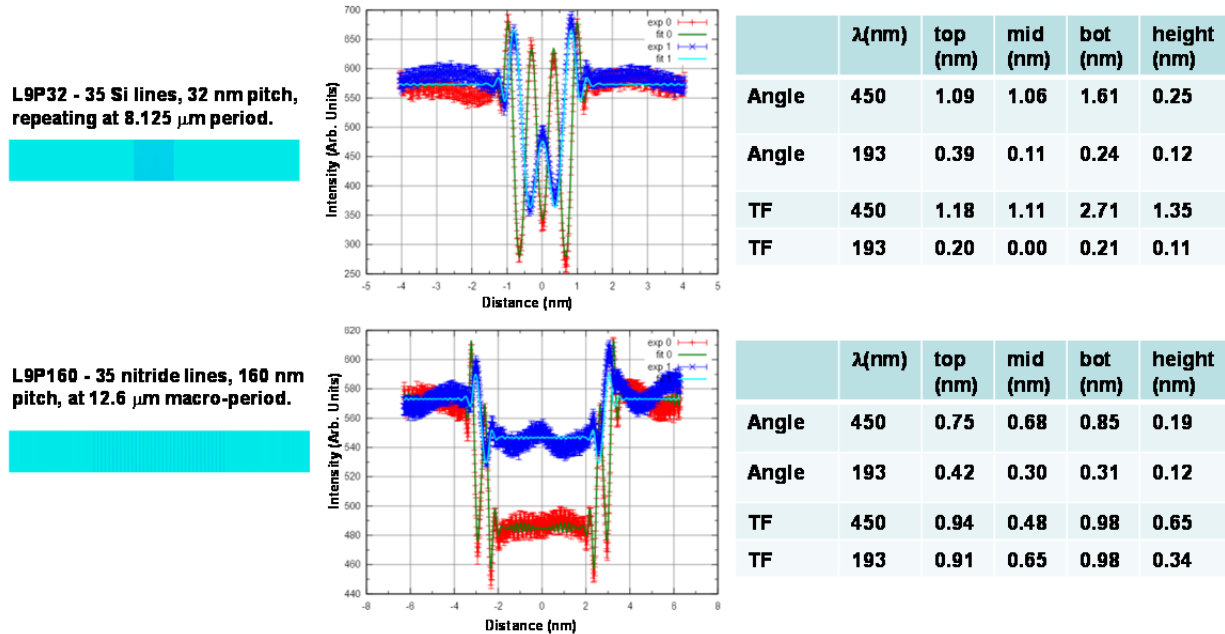


Figure 4. Simulation studies of 9 nm lines in dense and isolated line arrays. 82 profiles are used for each set of angle-resolved or focus-resolved data sets. The graphical images in the center each show best fit simulation curves and “simulated experimental curves” for two polarizations at a selected focus or angle position. Uncertainty is reduced with shorter wavelengths.

The uncertainties are again based on the noise profiles shown in the figure and are again realistic if not overly conservative. The challenge however as will be seen is that the noise must emulate the systematic modeling errors encountered in modeling as a result of the inherent requirement for accurate model parameters and methods.

One concern when measuring finite arrays as measured above is that the outer most edge may have an inordinately large affect on the scattered profile and potentially dominate the signal. This is not the case and the data show that the outer most edge has an effect approximately proportional to the number of lines that scatter high order light. On further investigation, the data show that in the middle of a sufficiently large array, a steady state scattered signal is achieved mid array, however, as one approaches the edge, the scattered light transitions from diffraction grating behavior to isolated feature behavior with a continuum of spatial frequency information. Additional study was undertaken to evaluate the effects of the outer lines and edges and to further understand the number of features required to obtain either grating like behavior or a target that contains significant high order optical content. Figure 5 shows an example of these data for angle- and focus-resolved acquisition with the decrease in uncertainties as the number of lines is increased resulting in a stronger optical signal sensitivity. These data show that the image content and frequency information is not dominated by the outer most features. There is a transition from an array optical response to more of an isolated feature behavior with broad optical content.

Angle-resolved					Focus-resolved				
# lines	top (nm)	mid (nm)	bot (nm)	height (nm)	# lines	top (nm)	mid (nm)	bot (nm)	height (nm)
5	0.69	0.51	0.68	0.19	5	2.18	1.77	2.63	0.58
10	0.64	0.40	0.46	0.19	10	1.69	1.28	1.80	0.50
15	0.57	0.35	0.40	0.17	15	1.41	1.01	1.36	0.44
20	0.50	0.31	0.34	0.15	20	1.15	0.79	1.02	0.37
25	0.46	0.28	0.31	0.14	25	1.00	0.67	0.83	0.33

Figure 5. “L9P32” - vary the number of Si lines of a 32 nm pitch, repeating at a 8 μm period on Si to determine the number of lines and edges required to obtain grating like behavior or to evaluate the enhanced optical signal strength and its effect on the uncertainty.

4. EXPERIMENTAL RESULTS

An experimental sensitivity analysis was carried out to validate and quantify the observed sensitivity as well as for subsequent theory to experiment comparisons. Accurate comparisons with minimal residuals are essential to develop quantitative modeling and an independent measurement capability. As mentioned in Section 1 two types of targets were measured, L100P600 that fills the entire field of view and the L100P300 and L50P175 targets both of which only partially fill the field of view.

The L100P600 targets are of particular interest as they contain only $m = -1, 0$ and $+1$ orders at normal incidence although the 2nd order can be rocked in at high angles. Figure 6 shows x and y polarization with several panels at varying focus slices. Each panel at a given focus position shows eight profiles plotted together that correspond to eight different CD values each acquired at a different die across a focus exposure matrix (FEM). For each polarization the figure shows ten sets of plots with each set of profiles acquired at focus positions from 400 nm above the substrate to 500 nm below substrate in 100 nm increments. The data show good sensitivity to the nanometer scale changes in linewidth for the focus-resolved experiments.

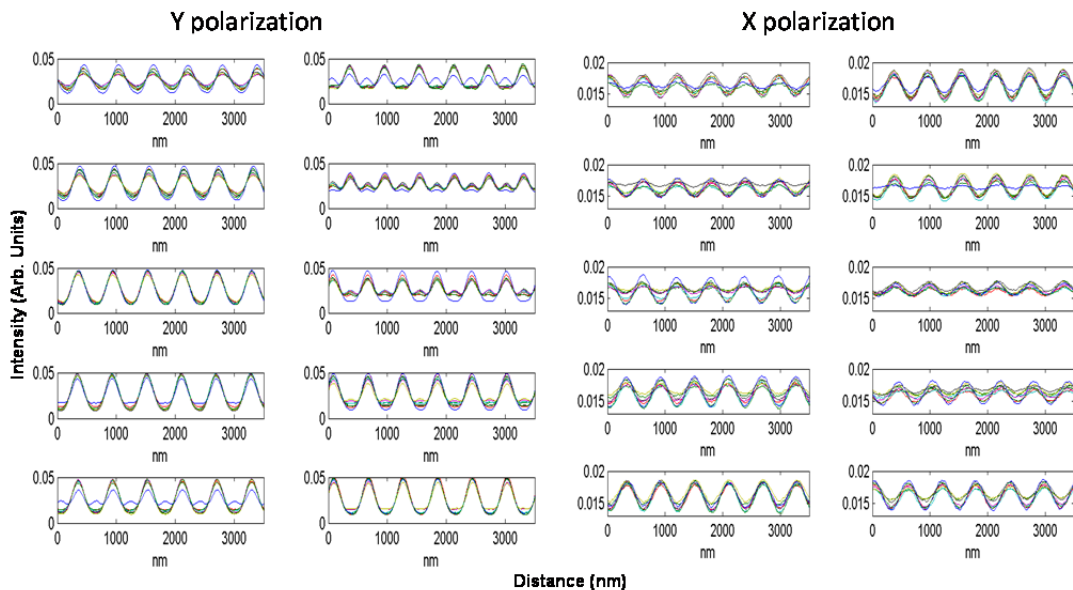


Figure 6. Experimental focus-resolved L100P600 lines. The left side and right side data sets show profiles acquired from 400 nm above the substrate to 500 nm below in 100 nm increments.

Enlargements of the best focus panels from Figure 6 are shown in Figure 7, where the profiles from the eight die can be resolved. The σ_{repeat} values in the figure are the range of repeatabilities for each data point scaled to the figures as labeled. The FEM resulted in the eight die having a nominal variation in middle linewidth of 10 nm ranging from 115 nm to 125 nm and sidewall variations of ranging from 5° to 8°.

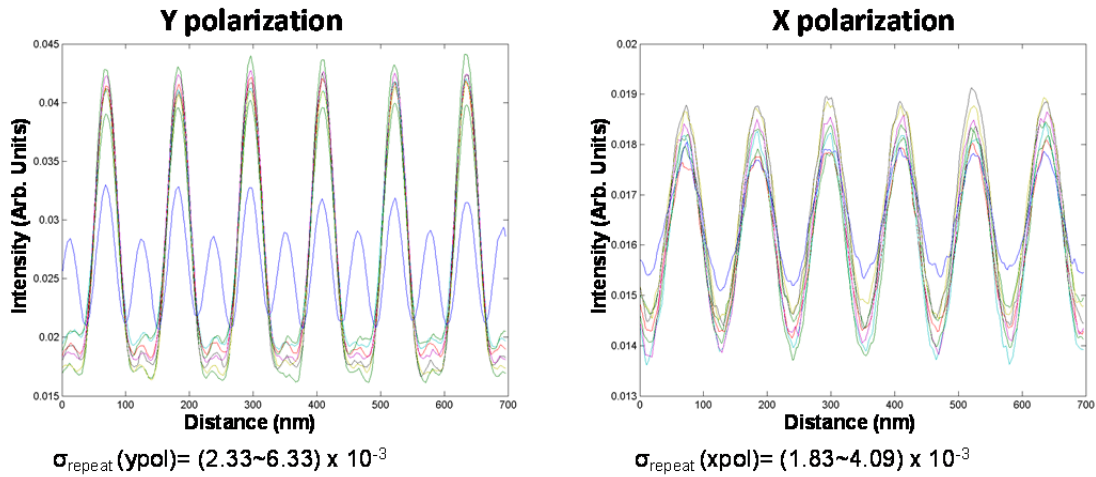


Figure 7. Experimental focus-resolved data from Figure 6. The figure shows a zoom in from the best focus panel above.

In Figure 8, the two graphs show sets of image profiles acquired at a given angle and at best focus, each showing eight profiles for the eight die. The σ_{repeat} values are again the range of repeatabilities for each data point scaled to the figures as labeled and the eight die are the same as used for the L100P600 data above. Again, very good sensitivity is seen to the linewidth variations as a function of angle.

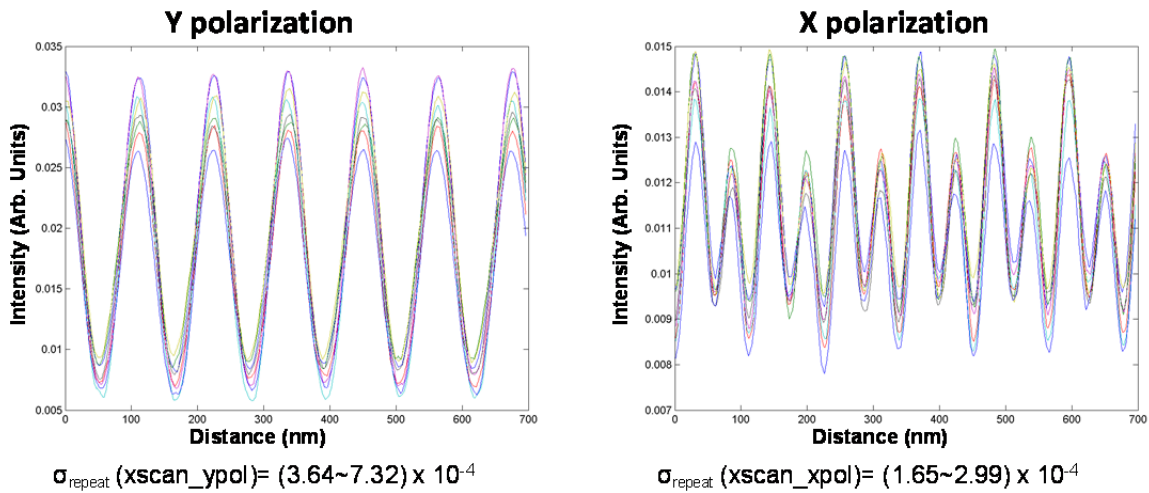


Figure 8. Experimental angle-resolved data showing profiles from eight die in each panel acquired at best focus and near to on axis on the left and at high angle on the right.

Next, we present data from the L100P300 target. This target is measured such that the edge of a large array is positioned in middle of the field of view. Looking at the right side of Figure 9, the optical response to the edge is seen in the middle of the panel while the bare silicon substrate is seen on the left side of the edge. On the right side of the edge, the optical response or reflectivity to the different linewidths for each array varies similar to the specular reflection value in

scatterometry at a given angle and wavelength. On the left side of the figure, ten sets of plots are shown for the L100P300 edges at focus positions ranging from 400 nm above the substrate to 500 nm below the substrate in 100 nm increments. In each plot, eight profiles are shown together corresponding to eight different CDs from different die.

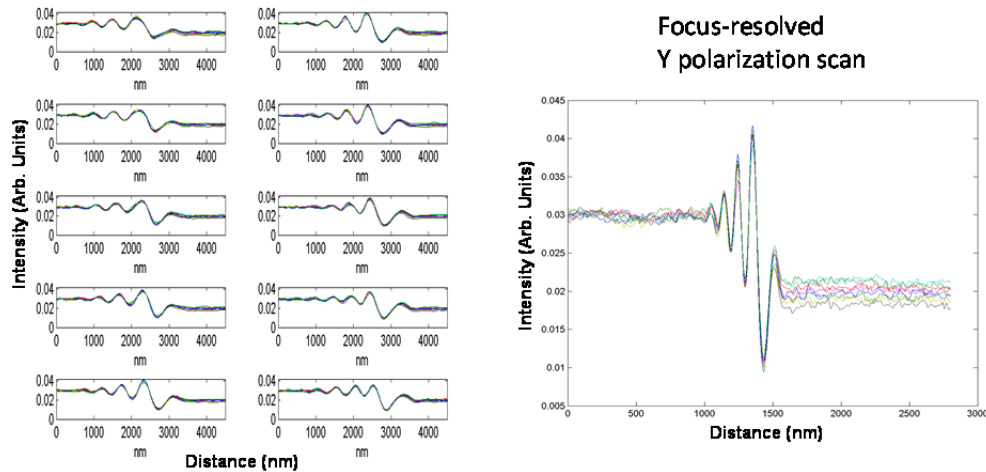


Figure 9. Experimental focus-resolved data for the L100P300 edge. The figure on the right shows a zoom in from one panel on the left.

Figure 10 shows angle resolved data from the L100P300 target. This target is again measured such that the edge of a large array is positioned in middle of the field of view and on the right side of the figure the optical response to the edge is seen in the middle, the bare silicon substrate on the left, and on the right side of the edge, the optical response to the different linewidths. On the left side of the figure, 16 sets of y scan x polarization plots are shown for the L100P300 edges as a function of illumination angle ranging from -32° to 32° . In each panel eight profiles are shown together corresponding to eight different CDs from different die.

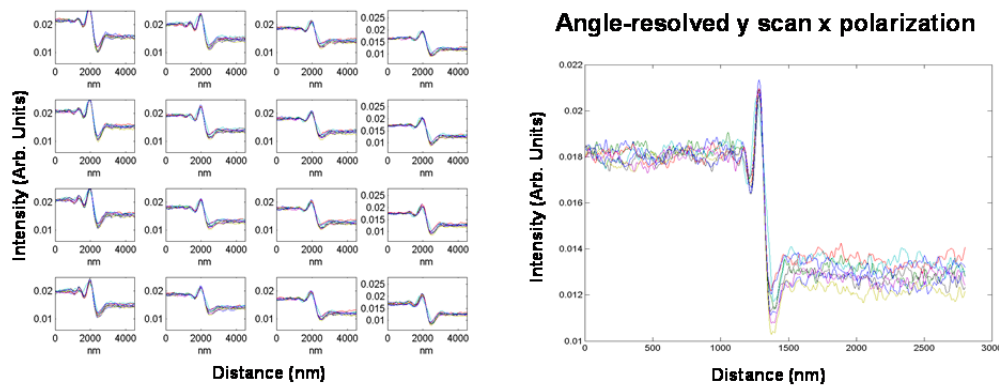


Figure 10. Experimental angle-resolved data for the L100P300 edge. The figure on the right shows a zoom in from one panel on the left.

Figure 11 shows angle resolved data from the L50P175 target. This target is again measured with the array positioned in middle of the field of view and in the figure on the right side, to the right of the edge the optical response to the different linewidths is shown for nitride lines on silicon. On the left side of the figure, 16 sets of plots are shown for the L50P175 edges as a function of illumination angle ranging from -32° to 32° . Eight profiles are shown together corresponding to eight different CDs ranging from 35 nm to 40 nm nominal width with incident angles from -32.5 to 32.5 degrees.

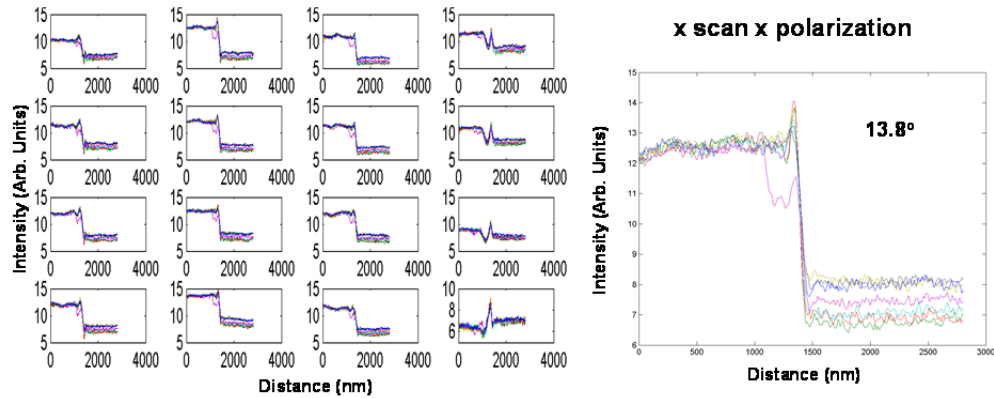


Figure 11. Experimental angle-resolved data for the L50P175 array edge. The figure shows a zoom in from one panel on the left.

5. ADVANCED TOOL CHARACTERIZATION

Before comparing experimental results with simulation, the experimental data needs to be “normalized” or corrected for instrumentation and hardware errors. To implement accurate library-based fitting methods based on electromagnetic scattering simulations, proper experimental normalization procedures are needed to allow accurate comparison of angle-resolved or focus-resolved measurements with theory. In practice, this is very complicated when high order scattered light is involved since the tool function that corrects for the illumination path must be calculated and implemented separately from the tool function that is applied to the collection path.

This is different than previous work where a single corrected path was used for each illumination angle as light traversed the optics since there was no high order scattering and limited polarization mixing. This simplified example is described in Figure 12. Although described in depth in Ref. 3, a background is acquired for each image as a function of angle, either directly during image acquisition or at a nearby site. The angle-resolved background scan is then normalized using a known silicon reflectance. The image is then normalized to this background allowing the experimental data to be accurately compared to theory. Once the data are acquired and normalized, they can be analyzed using library-based fitting techniques.

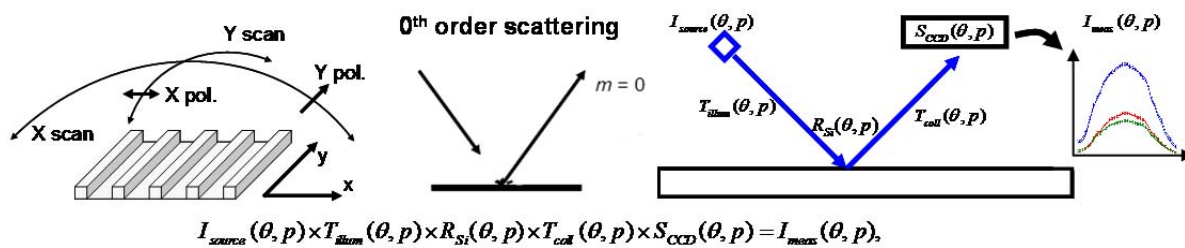


Figure 12. Schematic of the tool function for a specular reflection signal. A simplified tool function can be used. The scanning directions and polarization directions are defined on the left.

When high order light is scattered by the sample, the optical metrology tool paths must be characterized separately for illumination and collection as a single illumination angle results in a vast spectrum of scattered light. The tool must be characterized as a function of polarization and angle over the entire conjugate back plane. The actual acquisition of the tool function is accomplished by placing a detector and polarizer at the sample plane and acquiring intensities for x and y positions of the detector polarizer and the illumination polarizer. Then, a mirror or silicon surface is placed at the sample plane and the same four polarization states are acquired at the CCD image detector for the complete path. This is

shown schematically in Figure 13. The illumination function is then removed from the complete pass tool function arriving at a collection function. Great care needs to be taken to quantify and account for the off-axis behavior of the system, and this is particularly challenging as the detectors and polarizers have non-optimum behavior at oblique, off-axis incidence that is accentuated at high angles.

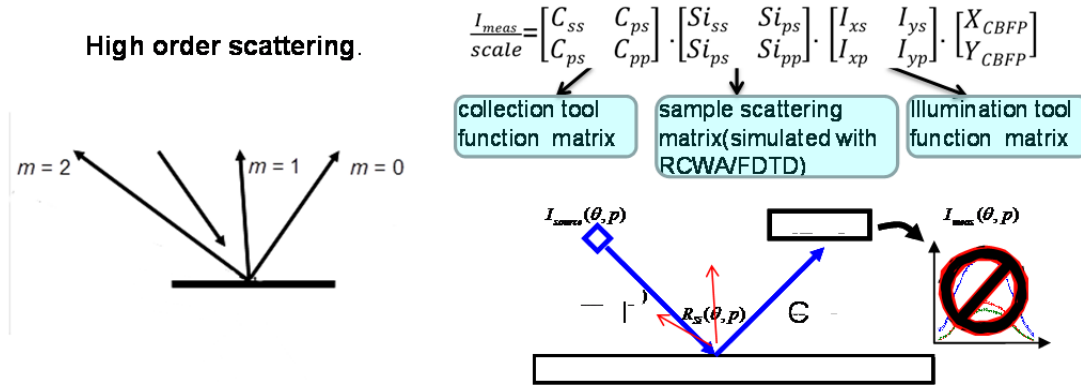


Figure 13. Method for tool normalization when high order scattered light is present. Both scattered light angles and polarization states need to be correctly normalized.

Once the illumination and collection functions have been acquired for the entire range of angles and polarization states, a new approach must be taken when applied to a sample that scatters high order light. A new Fourier front and back end was developed for our simulation code that allows the scattered light to be normalized in the frequency domain. The collection path normalization is accomplished by applying the tool correction to the scattered light as a function of scattering angle. The normalized light is then recombined at the image plane and an image is reconstructed.

6. THEORY TO EXPERIMENT COMPARISONS

In this section we show a comparison of experimental data with theoretical simulations. The example shown here is an L100P600 target that fills the field of view. Although the pitch and CDs are larger with this sample, it provides an important test of the modeling and normalization method as there is substantial through-focus phase contrast and intensity variation. In Figure 14 two polarizations are shown at normal incidence for three different focus positions. This uses the full Fourier normalization approach for the illumination tool function and the collection path applied to the scattered orders. Three slices of the fields are shown in 100 nm increments.

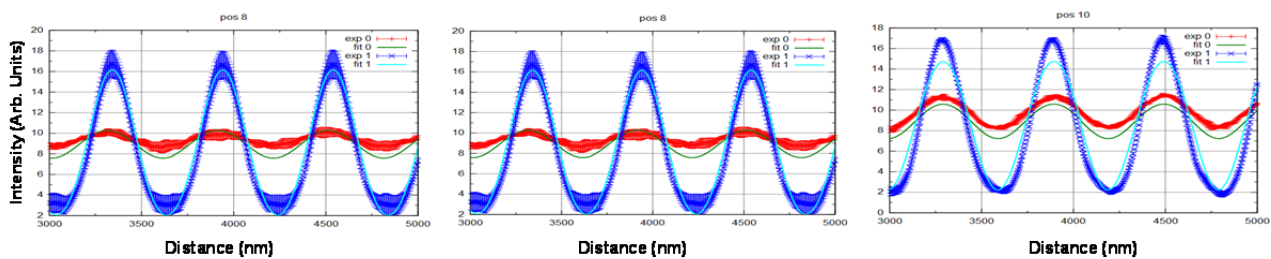


Figure 14. Focus-resolved theory to experiment comparisons of the L100P600 target. The focus was varied in 100 nm increments between panels. Two different polarizations are shown in each graph.

One significant challenge in this fitting process is that a finite aperture must be used to ensure enough plane waves are simulated which creates a realistic through focus interference effect. The intensity inversion and contrast fluctuations taper off after a few oscillations, and this behavior is correctly captured by using a sufficient number of plane waves in the incident illumination and a proper application of the through focus Fourier domain tool normalization.

7. CONCLUSION

Through-focus and angle-resolved Scatterfield microscopy was used to demonstrate sensitivity in measurements of dense line arrays with dimensions that result in only specular reflected light as well as targets with higher order diffracted light. The technique was applied to larger scatterometry arrays that fill the optical field of view and to smaller targets only partially filling the field of view, potentially enabling in-chip applications with reduced target size. This approach allows for parallel measurements of multiple targets with applications in both CD and overlay metrology.

To implement the simulation study we developed a new approach to concatenate image-based data and then performed the regression analysis using methods previously developed. The simulation study presented here used a realistic noise model in obtaining the fitting uncertainties. Although the random and high frequency noise components may be improved in practice, the low frequency errors due to underlying inaccuracies in the theory to experiment fits mandates the use of accurate noise models that account for these types of errors.

Using accurate background normalization and optical tool compensation, a path to quantitative modeling was demonstrated for the L100P600 target. A sophisticated approach applied in the Fourier domain that corrects independently for optical path errors in the illumination and collection path was outlined. It is important to note that attention needs to be paid to polarization effects, and the tool function needs to fully account for optical system errors throughout the angular spectrum.

Both the modeling and experimental data demonstrate that nanometer-scale measurements can be achieved using angle-resolved or focus-resolved scatterfield microscopy. Accurate modeling and library fitting, however, is challenging and requires further development. Although the data presented here show clear sensitivity to nanometer scale dimensional changes both in the experimental results and simulation studies, a comprehensive model-based analysis that enables a stand-alone measurement capability requires further work.

ACKNOWLEDGEMENTS

The authors would like to thank SEMATECH for wafer fabrication and measurement support. The authors wish to thank Thomas Germer for providing a 2-D RCWA code and are indebted to Nien-Fan Zhang for research in developing the regression analysis and Bayesian statistical methods.

REFERENCES

- [1] R. M. Silver, B. Barnes, R. Attota, J. Jun, M. Stocker, E. Marx, and H. Patrick, "Scatterfield Microscopy to Extend the Limits of Image-based Optical Metrology," *Applied Optics*, Vol. 46, 20, pp. 4248-4257 (2007).
- [2] H. Patrick, R. Attota, B. Barnes, T. Germer, R.G. Dixon, M. Stocker, R. M. Silver, and M. Bishop, "Optical Critical Dimension Measurement of Silicon Grating Targets using Back Focal Plane Scatterfield Microscopy," *J Micor/Nanolith., MEMS and MOEMS* 7(1), 0137011, (2007).
- [3] B. M. Barnes, L.P. Howard, J. Jun, P.Lipscomb, and R.M. Silver, "Zero-order imaging of device-sized overlay targets using scatterfield microscopy," *Proc. SPIE* **6518**, 65180F (2007).
- [4] R. M. Silver, N. F. Zhang, B. Barnes, H. Zhou, A. Heckert, R. Dixon, T. Germer and B. Bunday, "Improving optical measurement accuracy using multi-technique nested uncertainties," *Proc. SPIE* **7272**, 727202 (Mar, 2009).
- [5] R. M. Silver, R. Attota, M. Stocker, M. Bishop, J. Jun, E. Marx, M. Davidson, and R. Larrabee, "The Limits of Image-based Optical Metrology," *SPIE Vol. 6152 61520Z-1*, 2006.
- [6] R. M. Silver, R. Attota, M. Stocker, M. Bishop, L. Howard, T. Germer, E. Marx, M. Davidson, and R. Larrabee, "High-resolution Optical Metrology," *Proc. SPIE Vol. 5752 p. 67*, (2005).
- [7] D. M. Shyu, Y. S. Ku, and W. T. Hsu, "Angle-resolved scatterfield microscope for linewidth measurement," *Proc. Spie* **7272**, 72721L (2009).

- [8] R. Quintanilha, Y. Sohn, B. M. Barnes, L. Howard, and R. Silver, "Critical dimension measurements using a 193 nm scatterfield optical microscope," Proc. SPIE 7390, 73900S (2009).
- [9] R. M. Silver, N. F. Zhang, B. Barnes, H. Zhou, J. Qin, and R. Dixon, "Nested Uncertainties to Improve Measurement Accuracy," Proc. SPIE **7971**, 797116 (2011).
- [10] J. Neter, W. Wasserman, and M. Kutner, (1983), Applied Linear regression Models, Richard D. Irwin, Inc, Homewood, Illinois.
- [11] D. M. Bates, and D. G. Watts, (1998) Nonlinear Regression Analysis and Its Applications, Wiley, New York.
- [12] R. Dixon, J. Fu, N. Orji, R. Allen, and M. Cresswell, "CD-AFM Reference metrology at NIST and SEMATECH," Proc. SPIE Vol. 5752-32, (2005)
- [13] R. M. Silver, T. Germer, R. Attota, E. Marx, M. Davidson, B. Barnes, J. Jun, and R. Larrabee, "Fundamental Optical Critical Dimension (OCD) Limits: A Simulation-based Study," SEMATECH Tech. Transfer #06044749A-TR, May 2006.
- [14] M. G. Moharam, D. A. Pommet, E. B. Grann, and T. K. Gaylord, "Stable implementation of the rigorous coupled-wave analysis for surface-relief gratings: enhanced transmittance matrix approach," J. Opt. Soc. Am. A 12, 1077-1086 (1995).